INTEGRATION OF CFD INTO SYSTEMS ANALYSIS CODES FOR MODELING THERMAL STRATIFICATION DURING SFR TRANSIENTS

Thomas H. Fanning and Justin W. Thomas

Argonne National Laboratory, USA

Abstract

The whole-plant systems analysis code SAS4A/SASSYS-1 has been coupled with a computational fluid dynamics code to assess the impact of high-fidelity simulations on safety-related performance for a sodium-cooled fast reactor (SFR). With the coupled capability, it is possible to identify critical safety-related phenomenon that cannot be resolved accurately with existing tools. In this work, the impact of coupling is demonstrated by evaluating plenum thermal stratification during a protected loss of flow transient. Stratification is shown to significantly alter core temperatures and flows predicted during natural circulation conditions. Significant temperature and flow impacts were also observed in the secondary coolant system, suggesting that resolving thermal stratification has far-reaching impacts on the whole plant.

1. Introduction

Under the U.S. Department of Energy's Nuclear Energy Advanced Modeling and Simulation (NEAMS) Program, high-fidelity reactor integrated performance and safety codes (IPSC) are being developed[1] to exploit advances in computers and software tools in order to facilitate reactor design optimization, provide increased assurance of performance and safety characteristics, and reduce the need for large scale integral experiments needed to characterize or validate reactor performance. To support whole-plant safety analyses for realistic transients, an existing systems analysis capability has been coupled with a high-fidelity computational fluid dynamics (CFD) code to assess the impact of high-fidelity simulations on safety-related performance. In this report, impact of coupling is demonstrated by evaluating the conditions of thermal stratification during a protected loss of flow transient.

The potential impact of thermal stratification on natural circulation flow rates was highlighted in a recent comparative study between the SAS4A/SASSYS-1 safety analysis code used in the United States[2] and the CERES safety analysis code used by the Central Research Institute of Electric Power Industry (CRIEPI) in Japan.[3] The comparison was made for the purpose of verification of the CERES code and was based on analysis of the August 2006 design of the 4S concept. Comparisons of the full-flow steady-state conditions show very good agreement for both protected and unprotected loss-of-flow transients. However, beyond the initial parts of the transients, where natural circulation behavior begins to dominate, the results for temperature and flow begin to show differences.[4]

Thermal stratification in the outlet plenum has been identified as a potential contributor to the natural circulation flow discrepancies between the two codes. Incorrect predictions of intermediate heat exchanger (IHX) primary inlet temperatures affect the predictions of natural circulation flow rates in the primary loop as well as heat rejection rates to the intermediate loop. This, in turn, impacts peak coolant and fuel temperatures observed during the transient.

In order to better predict the conditions of thermal stratification during this transient, the whole-plant systems analysis capabilities of SAS4A/SASSYS-1 have been coupled to the commercial computational fluid dynamics code STAR-CD.[5] Using these coupled tools, it is possible to evaluate the influence of thermal stratification in the outlet plenum on the remainder of the primary system, including the effect on the temperatures in the core. Results of the analysis based on SAS4A/SASSYS-1/STAR-CD coupling are presented below.

2. Coupling

The PRIMAR-4 module of SAS4A/SASSYS-1 computes coolant pressures, flow rates, and temperatures in the primary and intermediate heat transport loops. Within a given time step, liquid flow rates and pressures are calculated first, taking into account changes in pressure and flow rates during the time step but ignoring temperature changes. Then, liquid temperatures are calculated. This separation takes advantage of the fact that single-phase liquid flow rates are more sensitive to pressure changes than temperature changes and provides an opportunity for coupling.

2.1 Strategy

Equations for hydraulic conditions in the primary and intermediate coolant loops are solved by a semi-implicit or fully implicit time differencing scheme in which pressures and flows for all connected compressible volumes and liquid flow segments are solved simultaneously. In SAS4A/SASSYS-1, *compressible volumes* are used to represent large volumes using a perfect mixing model. *Liquid segments* are composed of *liquid elements* that represent specific components in the coolant loop. The coefficients to the equations are unique for each compressible volume and liquid flow element type. This allows a wide variety of system components to be modeled.

The momentum equation for single-phase incompressible liquid can be integrated over a liquid flow segment and summarized as

$$\frac{L}{A}\frac{dw}{dt} = f(w,t)$$

$$= p_{in}(w,t) - p_{out}(w,t)$$

$$-\Delta p_{fr}(w,t) - \Delta p_{w^2}(w,t) - \Delta p_{v}(w,t) - \Delta p_{er}(w,t) + \Delta p_{n}(w,t)$$
(1)

where w is the flow rate (kg/s), L is the length of the flow segment and A is the cross sectional area. Changes in flow are driven by the differences in inlet and outlet pressure balanced by friction, form, and valve pressure losses along with gravity and pump heads, respectively.

Inlet and outlet pressures for a liquid segment are determined by the properties and conditions of the compressible volumes connected at each end. Pressure in a compressible volume is assumed to vary linearly with changes in the mass or temperature of the liquid. Therefore, changes in the pressure of a compressible volume at a reference location can be written as

$$\Delta p_r = B_0 + B_1 \left(\sum \overline{w}_{in} - \sum \overline{w}_{out} \right) + B_2 \left(\sum \overline{w}_{in} T_{in} - \sum \overline{w}_{out} T_{out} \right), \tag{2}$$

where \overline{w}_{in} and \overline{w}_{out} are the individual inlet and outlet flow rates of each connected segment averaged over the time step. The coefficients B_0 , B_1 , and B_2 are defined based on the properties of the compressible volume and include the effects of liquid compressibility, liquid and vessel wall thermal expansion, vessel expansion due to internal pressure, cover gas expansion or contraction, and external heat sources or sinks. Some of these effects are extremely difficult to represent with existing CFD tools. Because of this, reference pressure calculations in the coupled solution are solved by SAS4A/SASSYS-1, but two important corrections are considered.

In the perfect mixing model used by SAS4A/SASSYS-1, the temperature of any coolant flowing out of the compressible volume is simply the mixed mean temperature of the volume. In Equation (2), T_{out} would be the same for all out-flowing connections. By eliminating the perfect mixing assumption and using a coupled CFD solution, however, T_{out} is unique for each outlet connection and will likely be different than the mixed mean. By taking this into consideration, the energy balance within the compressible volume will be more accurately resolved and the change in pressure during the time step will be more accurately predicted.

The second correction involves the calculation of p_{in} and p_{out} for Eq. (1). Under the assumptions of a perfect mixing model, the inlet pressure is calculated by

$$p_{in} = p_r + \rho_{mm} g(z_r - z_{in}),$$

where ρ_{mm} is the density of the coolant at the compressible volume mixed mean temperature, g is the acceleration due to gravity, z_r is the elevation of the reference pressure location, and z_{in} is the elevation of the inlet. With the coupled CFD solution available, a more detailed temperature and density distribution is known. Therefore, the inlet pressure used in the momentum equation can be more accurately defined:

$$p_{in} = p_r + g \int_{z_{in}}^{z_r} \rho(T) dz$$

In practice, the CFD solution calculates both the static head due to gravity and the dynamic pressure drop due to flow. For large volumes such as reactor outlet plenums, dynamic pressure is negligible compared to static pressure. Nevertheless, both contributions are included, and the inlet pressure for the coupled solution is calculated as

$$p_{in} = p_r + \Delta p_{CFD}$$

where Δp_{CFD} is the pressure difference in three-dimensional space calculated by CFD between the inlet and the reference locations. A similar treatment is used for outlet connections.

2.2 CFD Implementation

In order to couple with SAS4A/SASSYS-1, customization of STAR-CD is implemented via user subroutines that access an application-programming interface to modify the normal runtime behavior of the STAR-CD code.

Typically, the time step size required by CFD is smaller than that required by the SAS4A/SASSYS-1 code. STAR-CD employs an implicit time step scheme, so the time step size is limited by accuracy rather than stability. SAS4A/SASSYS-1 provides the beginning and end

time for a subinterval to STAR-CD. STAR-CD then iterates using a default user-supplied time step size and interpolates the SAS4A/SASSYS-1 temperature and flow data to evaluate boundary conditions for intermediate time steps. On the final STAR-CD time step within the larger subinterval, it may be necessary to adjust the STAR-CD time step size in order to synchronize.

The CFD simulations presented here were performed utilizing four cores of single node on a Linux cluster. Because such a simulation does not require network communication, this permits good scalability for a small CFD model. In the STAR-CD parallel implementation, the root process is responsible for all communication with SAS4A/SASSYS-1. The root process must then broadcast data read from SAS4A/SASSYS-1 to all other processes using MPI functions, which would require network communication for larger multi-node simulations. Conversely, in order to calculate the pressure and temperature at the boundaries for SAS4A/SASSYS-1, contributions from each process must be collected on the root via an MPI reduction operation. This implementation has the advantage of simplifying the procedure for synchronizing with SAS4A/SASSYS-1 and is consistent with the internal I/O procedure in STAR-CD. The additional overhead required to perform the MPI broadcast and reduction operations are negligible.

3. Coupled Model Description

Analysis of the protected loss-of-flow (PLOF) accident sequence for the 4S was performed with the coupled heat transfer, thermal-hydraulics, and reactor kinetics models available in the SAS4A/SASSYS-1 code. The PLOF accident begins with a loss of normal power to the primary, secondary, and feedwater coolant pumps due to a loss of the internal power supply (station blackout). This results in an immediate loss of forced flow in the primary and secondary coolant circuits. Equipment that provides a programmed flow coast down of the primary reactor coolant pumps is assumed to operate, and the flow coast down of the primary pump is assumed to follow a 15 second initial halving time. Secondary pump flow is assumed to stop immediately. When primary pump power reaches 80%, a reactor scram interlock signal will occur, and the reactor will scram following a short delay to account for response time.

Adiabatic conditions are assumed at the steam generator due to the water supply pump trip. As a result, the only heat removal during the transient is through the reactor vessel auxiliary cooling system (RVACS) and the intermediate reactor auxiliary cooling system (IRACS).

In the PLOF sequence, the absence of normal shutdown heat removal through the reactor coolant system causes a slow system temperature rise following the reactor scram. This temperature increase occurs because the RVACS and IRACS have insufficient heat removal capacity to overcome both the early decay heat production rate and the stored heat in the primary and secondary systems. Eventually, the decay heat will fall below the emergency cooling capacity, and the system temperature will decline.

3.1 Primary and Secondary System Modeling

In the SAS4A/SASSYS-1 code, individual channels are used to represent the core, while the PRIMAR-4 module treats the primary and secondary sodium loops, as well as the steam generator. A simplified representation of the 4S primary system is shown in Figure 1 (left). The secondary system and steam generators are not shown.

The outlet plenum of the 4S is approximately eleven meters tall. A simplified three-dimensional surface representation of the outlet plenum is shown in Figure 1 (right). From the core outlet elevation (red surface) to the IHX inlet elevation (green surface) is approximately 7.7 meters. There is an annular wall that extends 0.58 meters above the elevation of the IHX, so coolant must first travel vertically at least 8.3 meters before dropping into the IHX inlet.

SAS4A/SASSYS-1 can approximate the outlet plenum by a compressible volume with a perfect mixing model. During higher flow conditions, this treatment is adequate and comparisons between SAS4A/SASSYS-1 and CERES have shown good agreement during the initial part of the PLOF transient. At later times, however, significant differences occur due to the inability of the simplified SAS4A/SASSYS-1 compressible volume model to treat the low-flow thermal stratification that occurs.

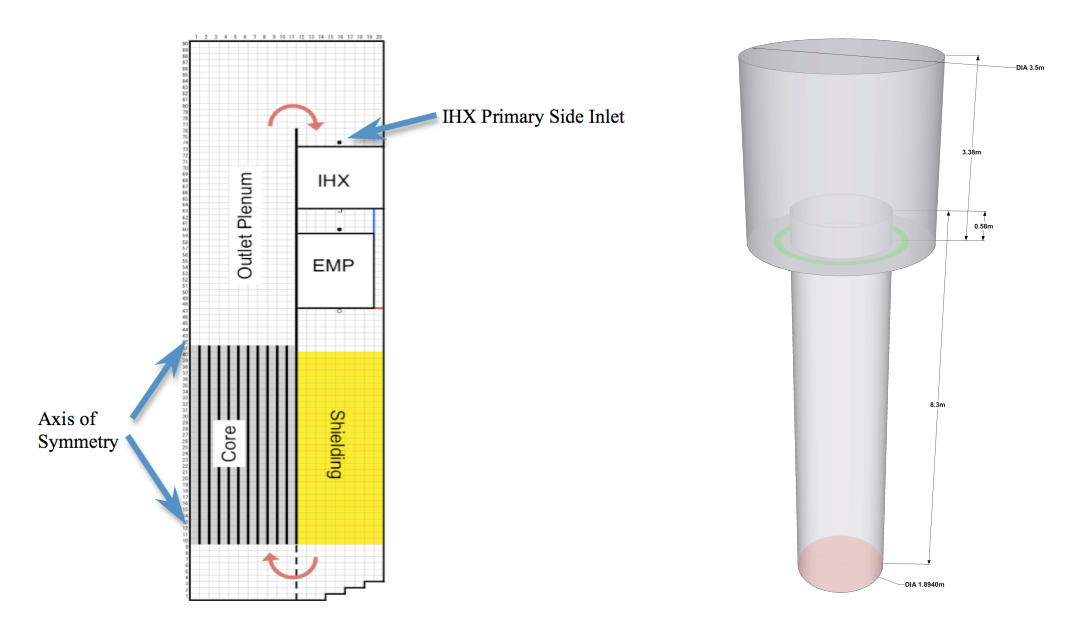


Figure 1: Simplified Representation of the 4S Primary System (left) and Three-dimensional surface representation of the 4S outlet plenum (right).

Details of the core outlet (in red) are excluded.

3.2 CFD Model

The STAR-CD model employed for the SAS4A/SASSYS-1 coupling demonstration is a two-dimensional, single-phase, axisymmetric model. The conclusion from previous work[6] was that the results from this simple, faster-running model were nearly identical to the more sophisticated models tested. Thus, it provides a good starting point for the development of more sophisticated coupling techniques with SAS4A/SASSYS-1. The grid for the axisymmetric model contains 29,000 cells. The temperature dependence of sodium thermo-physical properties is evaluated using the same expressions used in SAS4A/SASSYS-1 and is implemented via user subroutines.

Sensitivity analyses were performed with STAR-CD running in standalone mode in order to evaluate the impact of time-step size on the solution. Calculations were performed with varying time step sizes from 0.01 to 0.05 seconds. For these sensitivity analyses, the boundary conditions for the core channel outlets were taken from earlier SAS4A/SASSYS-1 analyses reported in [6].

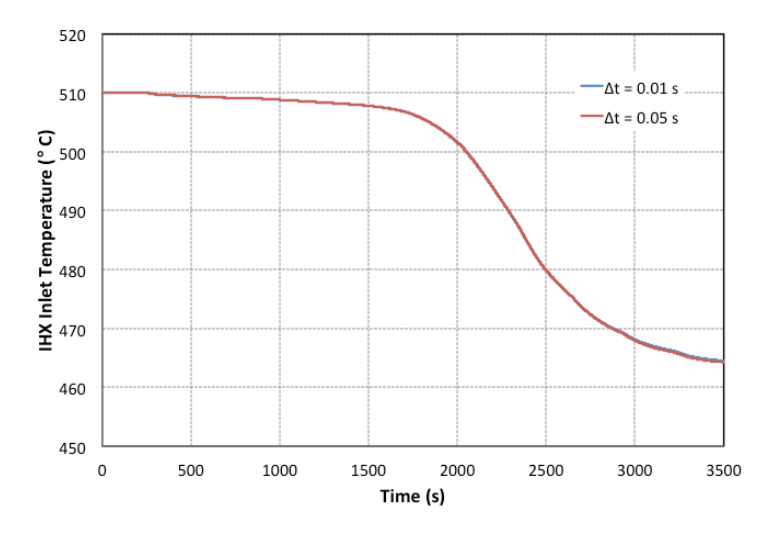


Figure 2: STAR-CD Time Step Size Sensitivity Study Results

The evolution of the IHX inlet temperature from the sensitivity analysis is plotted in Figure 2. Based on this analysis, there is no appreciable difference between the two time step sizes and the larger 0.05-second time-step size is used for subsequent analyses.

4. Coupled Model Results

Two simulation results are compared. In one case, a "one-way" coupling was carried out in which data was sent from SAS4A/SASSYS-1 to STAR-CD, but data returned to SAS4A/SASSYS-1 was not used in the whole-plant simulation. In this case, the SAS4A/SASSY-1 results are identical to an uncoupled calculation, and the STAR-CD results are based on uncoupled boundary conditions. For the coupled results, temperature, pressure, and flow coupling is carried out as describe above.

Simulations were performed on a quad-core machine and required approximately 39 hours of wall clock time. Nearly all of the computational burden is associated with the CFD simulation of the plenum. The long run time is primarily associated with the long length of the transient; the 4200-second transient (800-second null transient and 3600-second transient) required 84,000 CFD time steps. Some of the computational burden may be alleviated by employing workstation machines with more cores — avoiding network communication while still reducing the size of the computational domain — or by improving the temporal discretization.

Because the results below are based on a conceptual design, validation of the system performance cannot be carried out. Of particular interest, however, is the *impact* that high-fidelity treatment of a particular phenomenon can have on whole-plant performance.

4.1 Steady-State Initialization

The CFD predictions for the initial condition of the plenum exhibit the expected behavior. Temperature distributions, velocity magnitude, and pressure for the one-way and fully coupled results are shown in Figure 3. Heat is transferred quickly from the core plume to the region above the reflectors, yielding a fairly short thermal entrance region. Near the plenum walls, the velocity magnitude is quite small, and the core plume moves towards the interior of the plenum.

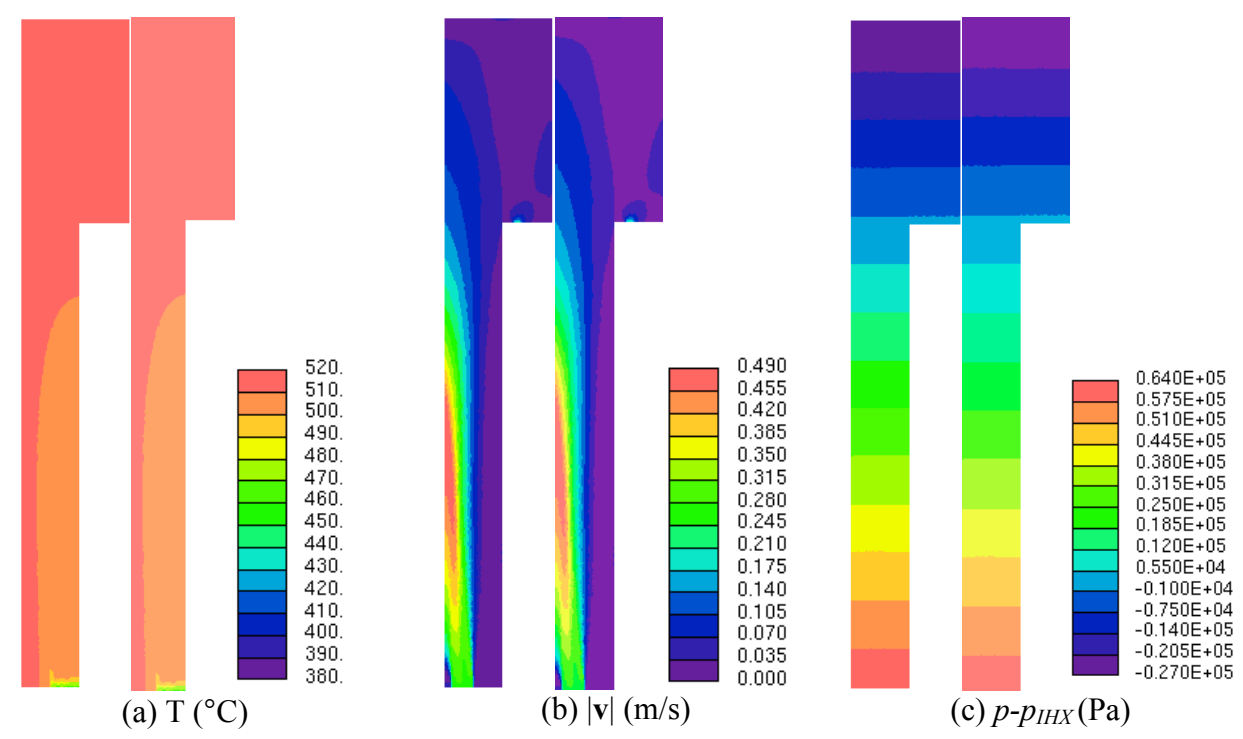


Figure 3: STAR-CD Predictions for (a) Temperature, (b) Velocity Magnitude, and (c) Pressure at t = 0 for Uncoupled (left) and Coupled (right) Cases.

As expected, pressure varies linearly with elevation, as gravity head is dominant and dynamic pressure is negligible.

4.2 Transient Results

4.2.1 Outlet Plenum Temperature Distributions

The STAR-CD predictions for the outlet plenum temperature distributions are shown in Figure 4. At 2000 seconds, the difference between the one-way coupling and fully coupled results is substantial enough to be seen in the contour plots. From the SAS4A/SASSYS-1 results, the deviation exceeds 10°C at approximately 1500 seconds. The vicinity of the IHX inlet appears cooler throughout the transient in the fully coupled case. In both cases, however, the temperature is much higher than in the perfect mixing model.

Some interesting phenomena can be noted from the coupled simulation. At 200 seconds, the temperature gradients in the lower section of the plenum are quite steep. By 500 seconds, thicker temperature layers develop. At 1000 seconds, the fluid in the lower section of the plenum is warmer than the fluid above it, because the core outlet temperature is rising relatively sharply. Cooler fluid reaches the annular region above the IHX between 1000 and 2000 seconds. In the natural circulation phase of the transient, the core outlet temperature reaches a peak at approximately 2000 seconds in the fully coupled case, and approximately 2700 seconds in the uncoupled case. Beyond this peak, there is a sharp gradient in the axial temperature profile close to the core outlet, but the mid-region of the plenum is fairly uniform. After 2700 s, the stratified layers exist primarily above the IHX inlet elevation.

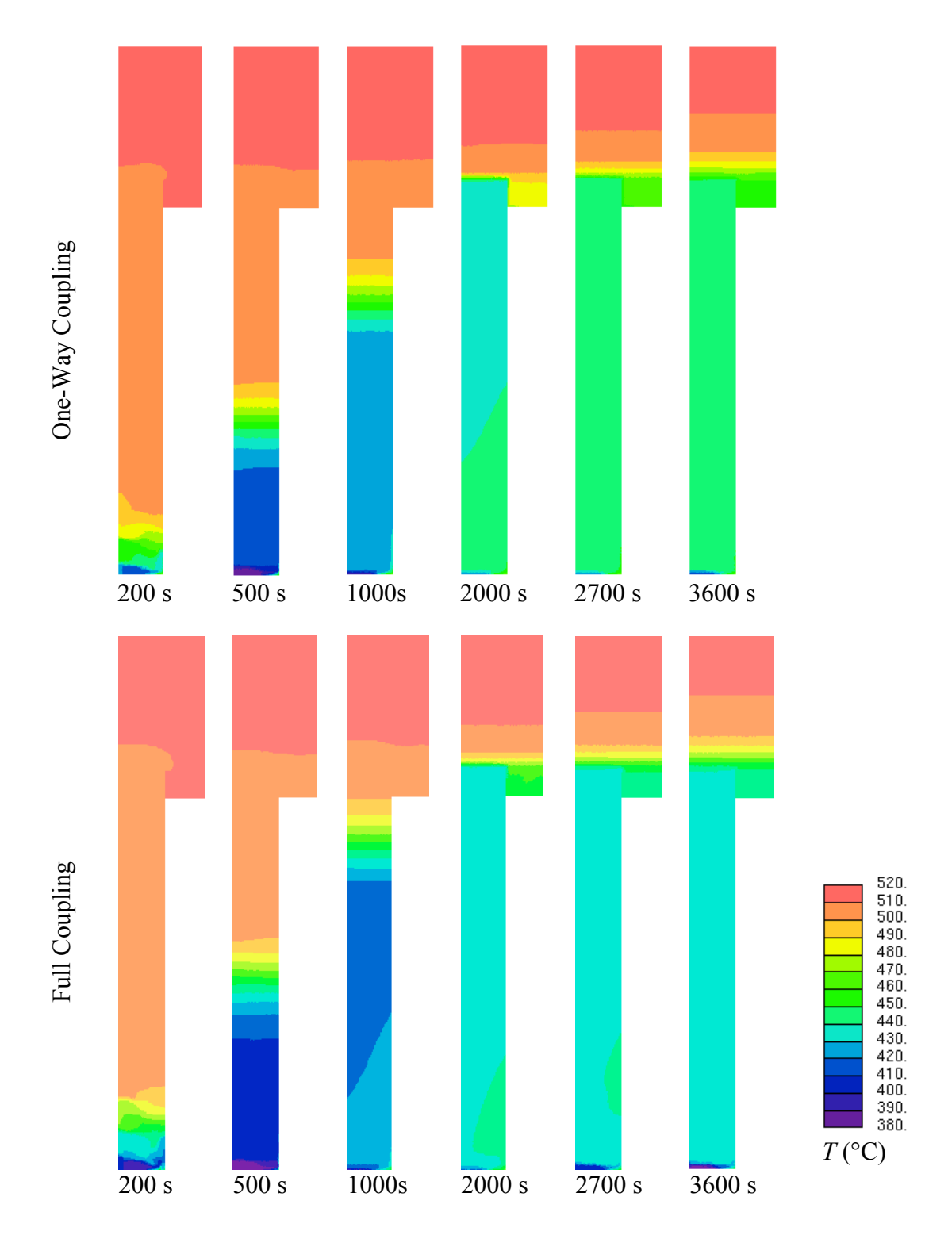


Figure 4: STAR-CD Prediction for Temperature Contours at Selected Times for One-Way Coupling (top) and Full Coupling (bottom) Codes.

4.2.2 IHX Temperature and Flow

IHX inlet and outlet temperatures for the uncoupled and coupled cases are shown in Figure 5. For the uncoupled results, the IHX intermediate- and primary-side outlet temperatures both increase during the early part of the transient due to loss of flow in both loops. The rapid reduction in power and flow on the primary side then causes the IHX primary-side outlet to reduce in temperature because of heat being transferred to the IHX intermediate-side. Over time, the intermediate system as a whole heats up and this heat transfer is reduced. Around 1200 seconds, the IHX is approximately isothermal.

Beyond 1200 seconds, intermediate system temperatures begin to decline due in part to an intermediate reactor auxiliary cooling system and in part due to cooling of the primary system by the reactor vessel auxiliary cooling system (RVACS). By 2800 seconds, the system has approached a nearly asymptotic cooling state and temperatures continue to steadily decline.

The coupled results show a far more complex behavior. During the early part of the transient, the trends for the cold legs of the IHX (primary-side outlet and intermediate-side inlet) are similar to the uncoupled results except that the primary-side outlet heats faster. The reason for this is clear when the primary-side inlet temperature is compared. Due to thermal stratification in the outlet plenum, the IHX primary-side inlet temperature stays elevated for an extended period of time and does not begin appreciable decline until around 1200 seconds. This is consistent with the CFD temperature distributions shown in Figure 4.

Between 1600 and 2000 seconds, an unusual increase in the primary-side outlet temperature is predicted. This phenomenon can be understood by considering the flow rates on both the primary and secondary side, which are shown in Figure 6. During this time, the primary-side flow rate has dropped to approximately 5%, resulting in longer transit times through the IHX. Even more significant, the secondary-side flow rate is stagnating during this time interval, with a minimum flow rate of 0.5% calculated at around 2300 seconds. At this point, the IHX is unable to reject heat to the intermediate system, and the hot coolant that had entered the primary side much earlier exits the primary side unchanged. The delay is also exaggerated due to the significant thermal inertia of the IHX structural components.

With heating of the IHX, natural circulation in the intermediate loop begins to increase slightly to a peak of approximately 1.5% shortly before 2800 seconds. This phenomenon seems to introduce a periodic behavior with multiple modes that depend on time constants in both the primary and intermediate systems.

Finally, because of the long initial heating period of the intermediate loop between 0 and 1400 seconds, the intermediate system becomes a heat *source* for the primary system rather than a heat sink. After 1600 seconds, coolant enters the intermediate-side of the IHX at a relatively high temperature and exits at a lower temperature. Furthermore, because of the significantly lower flow rates in the intermediate system, the IRACS may be ineffective as an emergency heat removal system, although higher overall temperatures may mitigate this. IRACS heat rejection rates were not compared in this initial analysis.

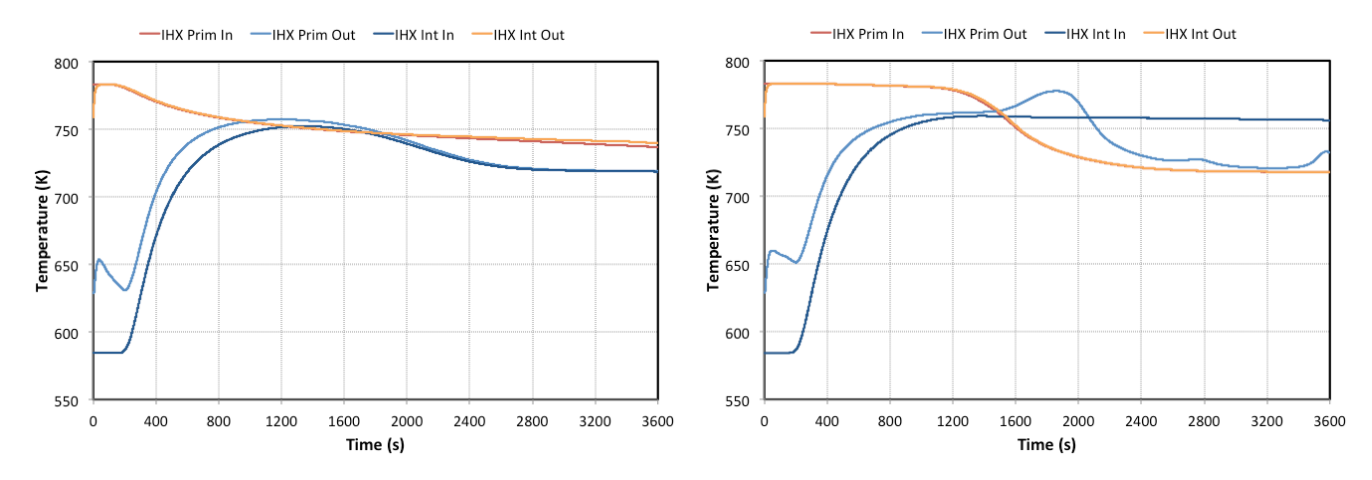


Figure 5: IHX Inlet and Outlet Temperatures for the Uncoupled (left) and Coupled (right) Cases.

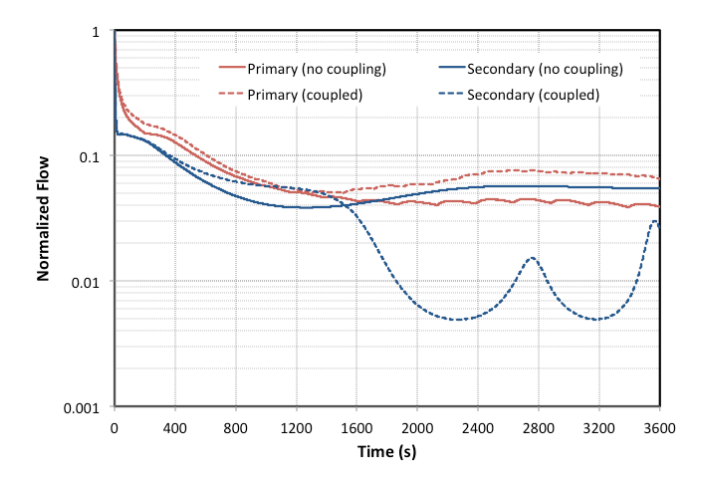


Figure 6: Normalized Primary and Secondary System Flow Rates for Both Coupled and Uncoupled Cases. Thermal stratification in the outlet plenum enhances primary system flow rates but causes flow stagnation in the secondary system.

4.2.3 Core Temperatures and Flows

Core inlet and outlet temperatures for the uncoupled and coupled cases are shown in Figure 7. The most obvious difference is that the peak core outlet temperatures for the coupled case occur earlier and at lower temperatures than the uncoupled case. In addition, core outlet temperatures decline faster after the peak is reached.

Differences in the inlet and outlet temperatures are plotted in Figure 8. During the early part of the transient (t < 400 s), there is a large transition in power and flow that leads to brief differences between the two temperature results. Since reactivity is dominated by the scram, power histories would be nearly identical. Both power and flow are changing rapidly during this time period. Slight differences in flow predictions may be contributing to outlet temperature variations. These differences are likely due to the initial development of thermal stratification in the outlet plenum.

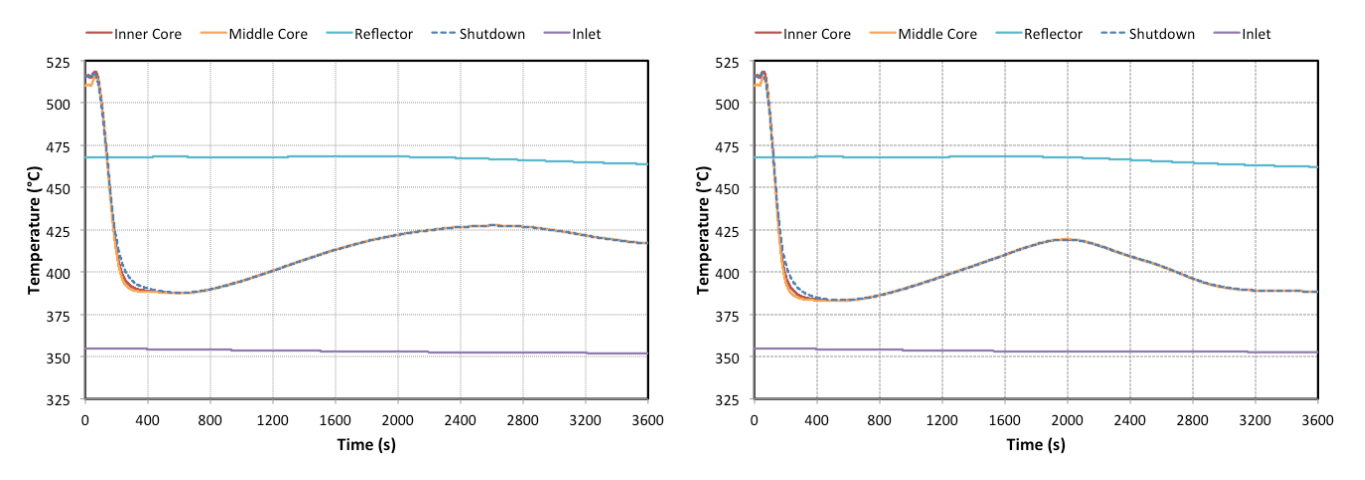


Figure 7: Core Inlet and Outlet Temperatures for the Uncoupled (left) and Coupled (right) Cases.

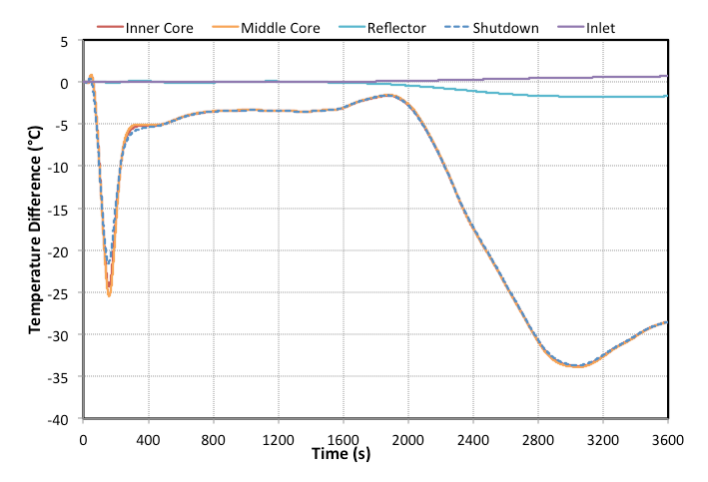


Figure 8: Core Inlet and Outlet Temperature Differences Between Coupled and Uncoupled Cases.

Between 400 and 2000 seconds, there is good agreement in the core outlet temperatures ($\Delta T < 5^{\circ}$ C). Beyond that time, however, the core outlet temperatures begin a faster decline in the coupled case than in the uncoupled case. This is due to a much faster rise in the natural circulation flow rates that develop in the latter parts of the transient when thermal stratification between the core outlet and IHX inlet has essentially ended (see Figure 4).

5. Summary

From the results of the SAS4A/SASSYS-1 analysis using either the perfect mixing or the three-tier thermal stratification model reported in earlier work, it is clear that such simple plenum models are insufficient to resolve the behavior of outlet plenum mixing and thermal stratification during a loss of flow transient where natural circulation is important. This work has demonstrated that with a proper coupling approach, a high-fidelity CFD tool can be used to resolve the important flow and temperature distributions in a reactor outlet plenum while still maintaining the whole-plant safety analysis capabilities of a systems analysis code.

Temperature and flow rate changes in the primary system and core were anticipated and observed as a result of resolving the thermal stratification in the outlet plenum. What was not anticipated, however, was the far-reaching impact that resolving thermal stratification would have on the whole plant. In the uncoupled case, the intermediate system acts as a heat sink for the duration of the simulation. In the coupled case, however, the high temperatures at the IHX inlet due to thermal stratification heat the intermediate system to the point that it eventually becomes a source of heat for the primary system. The results also suggest that flow stagnation in the intermediate system is possible, raising questions about the effectiveness of the IRACS during a protected loss of flow accident scenario.

Future application of these methods will include analysis of the Phénix end-of-life natural convection test that is part of an IAEA international benchmark and analysis of the EBR-II shutdown heat removal tests. In the case of the Phénix natural circulation test, a steam generator dry-out triggers a protected loss of flow sequence in which natural circulation provides core cooling. Thermocouple data in the outlet plenum is available for validation. In the case of EBR-II testing, thermocouple data shows thermal stratification in the cold pool during a variety of test sequences.

6. Acknowledgements

The submitted manuscript has been created by UChicago Argonne, LLC, Operator of Argonne National Laboratory ("Argonne"). Argonne, a U.S. Department of Energy Office of Science laboratory, is operated under Contract No. DE-AC02-06CH11357. The U.S. Government retains for itself, and others acting on its behalf, a paid-up nonexclusive, irrevocable worldwide license in said article to reproduce, prepare derivative works, distribute copies to the public, and perform publicly and display publicly, by or on behalf of the Government.

7. References

- [1] A. Siegel, T. Tautges, A. Caceres, D. Kaushik, and P. Fischer, "Software Design of SHARP," *Proc. Joint Int'l Topical Mtg. on Mathematics & Computation and Supercomputing in Nuclear Applications*, Monterey, California, April 15–19, 2007.
- [2] *The SAS4A/SASSYS-1 LMR Analysis Code System*, Volumes 1–5, ANL-FRA-1996-3, Argonne National Laboratory, August 1996.
- [3] Y. Nishi, N. Ueda, I. Kinoshita, A. Miyakawa, M. Kato, "Verification of the Plant Dynamics Analytic Code CERES using the Results of the Plant Trip Test of the Prototype Fast Breeder Reactor MONJU," *Proceedings of ICONE14*, Miami, Florida, July 17–20, 2006.
- [4] T. H. Fanning, F. E. Dunn, and Y. Nishi, "Development of 4S and Related Technologies: Comparison of Transient Accident Sequences Between the SAS4A/SASSYS-1 and CERES Reactor System Analysis Codes," *Proc. Int'l Congress on Advances in Nuclear Power Plants (ICAPP 2009)*, Tokyo, Japan, May 10–14, 2009.
- [5] STAR-CD Methodology Manual v4.12, CD-adapco Group, Melville, NY, 2010.
- [6] T. H. Fanning and T. Sofu, "Modeling of Thermal Stratification in Sodium Fast Reactor Outlet Plenums During Loss of Flow Transients," *Proc. International Conference of Fast Reactors and Related Fuel Cycles (FR 2010)*, Kyoto, Japan, December 7–11, 2009.